Hybrid convolutional neural network and projected entangled pair states wave functions for quantum many-particle states

Xiao Liang,[1] Shao-Jun Dong,[2,3] and Lixin He[2,3,*]

[1]*Institute for Advanced Study, Tsinghua University, Beijing 100084, China*

[2]*CAS Key Laboratory of Quantum Information, University of Science and Technology of China, Hefei 230026, Anhui, China*

[3]*Synergetic Innovation Center of Quantum Information and Quantum Physics, University of Science and Technology of China, Hefei 230026, China*

(Received 29 September 2020; revised 30 November 2020; accepted 5 January 2021; published 22 January 2021)

Neural networks have been used as variational wave functions for quantum many-particle problems. It has been shown that the correct sign structure is crucial to obtain highly-accurate ground state energies. In this paper, we propose a hybrid wave function combining the convolutional neural network (CNN) and projected entangled pair states (PEPS), in which the sign structures are determined by the PEPS, and the amplitudes of the wave functions are provided by CNN. We benchmark the ansatz on the highly frustrated spin-1/2 J_1-J_2 model. We show that the achieved ground energies are competitive with state-of-the-art results.

DOI: 10.1103/PhysRevB.103.035138

I. INTRODUCTION

Neural network (NN)-based machine learning (ML) has been applied to solve various physical problems [1,2], such as experiment automation [3], quantum state classification [4–8], emerging physics from neural networks [9], simulation of quantum computation [10], accelerating Monte Carlo calculations [11–13], accelerating density-functional-theory calculations [14,15], representing quantum states [16–25], and time evolution for open quantum systems [26–29].

Recently, neural networks have also been applied to solve quantum many-particle problems, which is one of the most interesting and challenging fields in condensed matter physics. A variational ansatz, namely, a restricted Boltzmann machine (RBM), has been demonstrated that can solve the nonfrustrated Heisenberg model to a high accuracy [25], that is comparable with the state-of-the-art methods. It has been argued that RBM [16,18] and a convolutional neural network (CNN) [30] can even represent quantum states beyond area law entanglement, and therefore have great potential to solve a large class of quantum many-particle problems.

Solving quantum frustrated models is an even more challenging problem for neural networks. Some of the authors first attacked the highly frustrated spin-1/2 J_1-J_2 model on the square lattice via CNNs [31]. They have obtained ground state energies that are lower than the string-bond-states method [32]. Later on, Choo *et al.* found that the ground energies can be significantly improved by introducing a prior sign structure before CNN and enforcing rotational symmetry [33]. However, in Ref. [33], the sign structures were artificially assigned based on the Marshall-Peierls sign rule (MPSR) [34]. Westerhout *et al.* investigated the learning ability for the sign structure and amplitudes of the wave functions of quantum frustrated systems, using supervised ML. It was concluded that while CNNs have no problem in generating the amplitudes of the wave function, the generation of a sign structure is very challenging, especially for frustrated systems [35]. Since the sign structure is a discontinued function with respect to spin configurations, it is difficult to present the sign structure and the amplitude of the wave function by a single NN. Szabó *et al.* introduced a CNN structure for quantum many-particle wave functions, in which the sign structure is represented by a single-layer CNN, and the amplitudes of the wave function are represented by a separate deep CNN [36].

On the other hand, the tensor network methods, e.g., the projected entangled pair states (PEPS) method [37–41], has achieved extremely high precision in solving the ground energies of quantum many-particle problems, especially for highly frustrated systems [42–47]. In principle, the PEPS can present any quantum state faithfully, provided the tensor bond dimension is large enough. However, the computational scaling is extremely high to contract a PEPS, especially for a PEPS with periodic boundary conditions (PBCs), which limits their applications.

In this paper, we propose a hybrid PEPS and deep CNN hybrid structure, which combines the two state-of-art techniques, as a variational ansatz for the quantum many-particle problems. For a given spin configuration, the corresponding coefficient is the product of the sign (+ or −) provided by PEPS (with a small bond dimension) and the magnitude provided by CNN. We first show that the MPSR can be rigorously represented by the PEPS even with a virtual bond dimension $D = 1$ on the square lattice. More complicated sign rules should be able to be represented by PEPS with a larger bond dimension. Another advantage of using PEPS to present the sign structure is that the PEPS can be optimized via the time-evolution method without sampling over the spin configurations, which may bypass the spin generation problem [35]. We benchmark the ansatz by calculating the spin-1/2

*helx@ustc.edu.cn

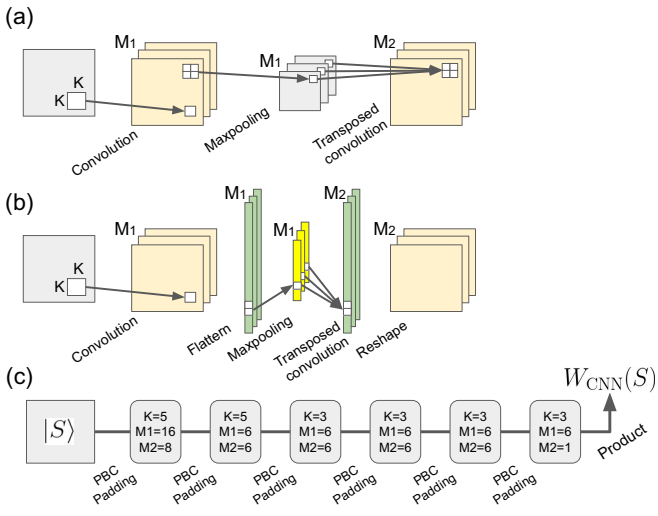

FIG. 1. Illustration of the deep CNN, where K is the side length of the convolution filter, and M_1 and M_2 are the output channels of convolution and transposed convolution, respectively. (a) The shallow CNN in Ref. [31]. (b) The building blocks for the deep CNN modified from the shallow CNN, in which the two-dimensional maxpooling and transposed convolution are changed to one dimensional. (c) The deep CNN is built by stacking the building block (b) for six times. To maintain the dimension, the input of each block is padded based on PBC. The input of the deep CNN is a spin configuration on the $|\sigma_1^z\sigma_2^z\cdots\sigma_N^z\rangle$ basis. The final output is denoted as $W_{\mathrm{CNN}}(S)$, and it is generated by taking the products of the output neurons in the last block.

J_1-J_2 model on the square lattice. We show that the sign rule provided by the PEPS can significantly improve the ground state energies of the J_1-J_2 model, which are very competitive with other state-of-the-art neural network wave functions. The results show that the PEPS + CNN hybrid structure is a very promising variational wave function for quantum many-particle problems.

II. METHODS

A. Deep CNN architecture

The building block of the deep CNN is based on the network used in a previous work [31], which is depicted in Fig. 1(a). Each block consists of a convolution layer, a maxpooling layer, and a transposed-convolution layer. In the figure, K denotes the convolution filter size, and M_1 and M_2 are the channel numbers of convolution and transposed-convolution respectively. To reveal the details of the CNN structure, we take a four-site spin chain as an example. We use $M_1 = M_2 = 1$ and $K = 3$. The convolution layer performs the following transformation,

$$\begin{bmatrix} p_1 \\ p_2 \\ p_3 \\ p_4 \end{bmatrix} = \mathbf{b} + \begin{bmatrix} w_1 & w_2 & w_3 & 0 & 0 & 0 \\ 0 & w_1 & w_2 & w_3 & 0 & 0 \\ 0 & 0 & w_1 & w_2 & w_3 & 0 \\ 0 & 0 & 0 & w_1 & w_2 & w_3 \end{bmatrix} \begin{bmatrix} s_4 \\ s_1 \\ s_2 \\ s_3 \\ s_4 \\ s_1 \end{bmatrix}, \quad (1)$$

where w are the weights of the filter, $\mathbf{b}$ is the bias vector, and $[s_4, s_1, s_2, s_3, s_4, s_1]^{\mathsf{T}}$ is the input spin configurations with $s_i = \pm 1$. To maintain the dimension, each side of the input is padded $(K-1)/2$ sites according to PBC.

Then maxpooling is performed on the neurons,

$$\begin{bmatrix} g_1 \\ g_2 \end{bmatrix} = \begin{bmatrix} \max(p_1, p_2) \\ \max(p_3, p_4) \end{bmatrix}. \quad (2)$$

After the maxpooling, a transposed convolution is performed,

$$\begin{bmatrix} h_1 \\ h_2 \\ h_3 \\ h_4 \end{bmatrix} = \begin{bmatrix} d_1 & 0 \\ d_2 & 0 \\ 0 & d_1 \\ 0 & d_2 \end{bmatrix} \begin{bmatrix} g_1 \\ g_2 \end{bmatrix}, \quad (3)$$

to restore the original size of the lattice.

Each output channel after transposed convolution is a direct summation of the neurons from each filter [31]:

$$\begin{bmatrix} h_1 \\ h_2 \\ h_3 \\ h_4 \end{bmatrix} = \sum_{m=1}^{M} \begin{bmatrix} d_1^{(m)} g_1^{(m)} \\ d_2^{(m)} g_2^{(m)} \\ d_3^{(m)} g_3^{(m)} \\ d_4^{(m)} g_4^{(m)} \end{bmatrix}. \quad (4)$$

For a two-dimensional (2D) spin lattice, the filters are 2D and the convolutions are performed in 2D. In the previous literature [31], the maxpooling and transposed convolution is chosen naturally as two dimensional, as shown in Fig. 1(a). However, because two-dimensional maxpooling neglects too many neurons, it reduces the representation ability when the CNN is deep. To build a deep CNN structure, we modify the two-dimensional maxpooling and transposed convolution to one dimensional. The modified structure is shown in Fig. 1(b). To fit the one-dimensional maxpooling, the output neurons of each convolution filter is also flattened to one dimensional, and the output neurons after transposed convolution are reshaped to maintain the dimension. Figure 1(b) is the building block of our deep CNN. Each neuron after the transposed convolution is a linear combination of the spin values

$$h_i = \sum_{k=1\cdots N} A_{i,k}\sigma_k^z + c_i, \quad (5)$$

where $A_{i,k}$ is the real coefficient of spin σ_i^z in h_i and c_i is a real number.

The deep CNN is built by stacking the building block six times, as shown schematically in Fig. 1(c). The input of the first block is 2D spin configurations on the basis of $|S\rangle = |\sigma_1^z\sigma_2^z\cdots\sigma_N^z\rangle$, and the value of each spin σ_i is ± 1. To maintain the dimension, each channel of the input of each building block is padded $(K-1)/2$ sites according to the PBC, which is the same as the one-dimensional case. The output of the deep CNN is the wave-function coefficient $W_{\mathrm{CNN}}(S)$, which is the product of the output neurons in the final block. The wave function that the deep CNN represents is

$$|\Psi_{\mathrm{CNN}}\rangle = \sum_S W_{\mathrm{CNN}}(S)|S\rangle, \quad (6)$$

where $|S\rangle$ is the spin configuration. Because of the product of the output neurons from the last building block, the deep CNN

associates the spin configuration to the high order correlations between the spins,

$$W_{\mathrm{CNN}}(S) = \sum_{n_1 \cdots n_N} g(n_1 \cdots n_N; \sigma_1 \cdots \sigma_N) \sigma_1^{n_1} \cdots \sigma_N^{n_N}, \quad (7)$$

where the order number $\tilde{N} = n_1 + n_2 + \cdots + n_N \leqslant N$ and the coefficient g is given by the deep CNN. Because of the maxpooling, g also depends on the spin configurations [31].

The deep CNN structure used in this work has several important differences compared to the deep CNN structure used in Refs. [33,36]. First, the nonlinearity in our deep CNN is induced by the maxpooling, whereas in Refs. [33,36], the activation functions are used. The maxpooling picks up the most important degree of freedom in a convolution filter, which is similar to the coarse-grained process in a renormalization group theory [48].

Another important difference is that, traditionally, the output wave functions are taken as the exponential function of the NN [16–18,22,25], whereas in our construction, the wave function $W_{\mathrm{CNN}}(S)$ is generated by taking the products of the neurons from the last building block [31]. In our deep CNN, $W_{\mathrm{CNN}}(S)$ can be either positive or negative, which is crucial to represent the ground states of frustrated systems, using only real network parameters.

As discussed in Ref. [31], the representability of the CNN structure relies on whether it can capture the long-range spin correlations (or entanglement). For the shallow CNN shown in Figs. 1(a) and 1(b), the first convolution layer is vital to capture the long-range correlation, therefore the CNN filter should be as large as the lattice size or the correlation length [31]. However, in the deep CNN, the spins in different filters of front layers can be entangled via maxpooling and convolution in the deeper neural networks, therefore it can capture the long-range spin correlations efficiently with much smaller filters. This is similar to the renormalization process in the numerical renormalization group method [49]. The information is reused by stacking the building blocks, which can enhance the representation ability [30]. In our investigations, we fix the deep CNN structure as depicted in Fig. 1(c), where there are 3531 real parameters. This is compared to the shallow CNN used in our previous work [31], where $M_1 = 128$ and $K = 9$ filters were used, leading to 11 009 real parameters. Obviously, the deep CNN has much fewer parameters.

When using a (deep) CNN to represent the quantum many-particle wave functions, the wave functions consist of a sign structure and amplitudes. In many ML cases, especially for regression problems, the output is usually continuously distributed with respect to the continuous input. However, this may not be true for a quantum system. Taking the J_1-J_2 model as an example. It is known that when $J_2 = 0$, the ground state exactly obeys the MPSR, and that the sign of the wave function is $(-1)^{M_A}$ where M_A is the magnetization of the equivalent sublattice A. MPSR is a discontinuous function with respect to flipping spin configurations. Therefore, the sign rule is quite difficult to be presented by a single CNN [35] which must keep the amplitude smooth at the same time [36]. It has been demonstrated in Ref. [33] that an explicit preconditioning to the CNN wave function by a MPSR can significantly improve the ground state energies compared to those without the preconditioning, for the J_1-J_2 model. However, the sign rule is added *ad hoc* by hand in Ref. [33]. Later on, Szabó *et al.* introduced a separate single-layer CNN to represent the sign structure, which is optimized with fixed amplitudes. They obtained an accurate MPSR for both $J_2 = 0$ and $J_2 = 0.5J_1$ [36].

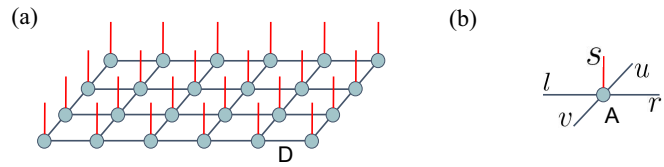

FIG. 2. (a) The illustration of a PEPS on a 4×6 lattice. The circles stand for a rank-five tensor on the lattice sites, which are connected by virtual bonds of dimension D. (b) The rank-five tensor $A(l, r, u, v, s)$ on each site has four virtual bonds, l, r, u, and v, and one physical index s.

B. PEPS-CNN hybrid structure

We propose a hybrid PEPS and CNN structure as a variational wave-function ansatz for the quantum many-particle problem. Considering a 2D square lattice with $N = L_x \times L_y$ sites, and d-dimensional local Hilbert space (for a spin-1/2 system, $d = 2$), denoted as $|s_m\rangle$ on the site $m = (i, j)$, the PEPS wave function of this system, which is schematically shown in Fig. 2(a), can be written as [39]

$$|\Psi_{\mathrm{PEPS}}\rangle = \sum_S W_{\mathrm{PEPS}}(S)|S\rangle, \quad (8)$$

where

$$W_{\mathrm{PEPS}}(S) = \mathrm{Tr}\left(A_1^{s_1} A_2^{s_2} \cdots A_N^{s_N}\right), \quad (9)$$

and $A_m^{s_m} = A_m(l, r, u, v, s_m)$ is a rank-five tensor located on site m as shown in Fig. 2(b). The physical index s_m takes a value from 1 to d and four virtual indices l, r, u, v, which correspond to four nearest neighbors. The dimension of each virtual bond is D, and the "Tr" denotes the contraction over all the virtual indices of the tensor network.

One way to construct the PEPS-CNN hybrid structure is to take the direct products of the PEPS wave functions to the CNN wave functions. Here, we propose an alternative PEPS-CNN hybrid structure as follows,

$$W(S) = \mathrm{sgn}[W_{\mathrm{PEPS}}(S)] \cdot W_{\mathrm{CNN}}(S), \quad (10)$$

i.e., we take the sign of the PEPS wave function and multiply it to the CNN wave function. We first show that the PEPS can rigorously represent the MPSR on the square lattice even with a virtual bond dimension $D = 1$. For both Néel order and stripe order, MPSR requires a spin flip on the sublattice, changing the wave function's sign. For $D = 1$, the PEPS on each site (i, j) only has two elements (a, b), one for spin up and one for spin down. For the Néel order, we take $a = 1$ for all sites and $b = (-1)^{i+j}$. For the stripe order, we take $a = 1$ for all sites and $b = (-1)^j$. One can easily prove that these PEPSs satisfy MPSR, which have also been checked numerically. One may expect that more complicated sign rules should be able to be presented by PEPS with larger D.

TABLE I. Comparison between the ground energies of the spin-1/2 J_1-J_2 model on a 10×10 square lattice, achieved by different CNN structures. "S. CNN" and "D. CNN" denote the shallow CNN and deep CNN, respectively.

	S. CNN	PEPS+S. CNN	PEPS+D. CNN
$J_2 = 0$	−0.668236	−0.670718	−0.671330
$J_2 = 0.5$	−0.482986	−0.492335	−0.495502

The ground state many-particle wave functions respect the symmetry of the Hamiltonian. We could therefore also enforce the rotational symmetry to the wave function [50],

$$\tilde{W}(S) = \sum_{i=0}^{3} W(\hat{T}^i S), \tag{11}$$

and $\hat{T}$ is the rotation operator that rotates the spin configuration for 90°.

III. RESULTS AND DISCUSSION

We benchmark the hybrid PEPS-CNN wave functions for the spin-1/2 J_1-J_2 model. The Hamiltonian of the model reads

$$\hat{H} = J_1 \sum_{\langle i,j \rangle} \mathbf{s}_i \cdot \mathbf{s}_j + J_2 \sum_{\langle\langle i,j \rangle\rangle} \mathbf{s}_i \cdot \mathbf{s}_j, \tag{12}$$

where $\langle i, j \rangle$ and $\langle\langle i, j \rangle\rangle$ indicate the nearest- and next-nearest-neighboring spin pairs. The model is calculated on a $L \times L$ square lattice with PBC. We set $J_1 = 1$ and $L = 10$ throughout the investigations and on two cases: $J_2 = 0$ and $J_2 = 0.5$. When $J_2 = 0.5$, the frustration is very strong and the ground state is inferred as the quantum spin liquid [51–53], therefore solving the ground state is challenging.

We first give the results of the shallow CNN used in the literature [31] without a prior sign structure but with enforcing rotational symmetry, for $J_2 = 0$ and $J_2 = 0.5$. The convolution filter numbers $M_1 = 128$ and $M_2 = 1$, and the side length of the filter $K = 9$, are used. The number of variational parameters of this NN is 11 009. The network is optimized by the stochastic reconfiguration (SR) method [54]. We obtain the energy per site −0.668 236 for $J_2 = 0$ and −0.482 986 for $J_2 = 0.5$, which are listed in Table I.

We then benchmark the shallow CNN multiplied by a prior sign structure provided by PEPS. We reduce the number of filters for the CNN structure to $M_1 = 90$ and $M_2 = 1$ with filter size $K = 9$. The total variational parameters of this structure are reduced to 7741 for the CNN. Since the computational scaling of a PEPS of PBC is very high, we use a PEPS with an open boundary condition, despite the physical system having a PBC. The PEPS bond dimension is taken to be $D = 1$, which allows the PEPS to be efficiently contracted.

To obtain the sign structure, we first optimize the PEPS wave function alone (without CNN) for $J_2 = 0$ using the imaginary time-evolution method with the so-called simple update scheme [39]. We exam the signs of the wave function on massive random spin configurations, and find that the sign rule provided by PEPS is consistent with MPSR. After we obtain the PEPS for the sign structure, the CNN wave function is then optimized with the SR method, by fixing the PEPS sign rules as a precondition factor. For $J_2 = 0$, the ground state energy is calculated to be $E = -0.670\,718$, which is significantly better than that without the precondition.

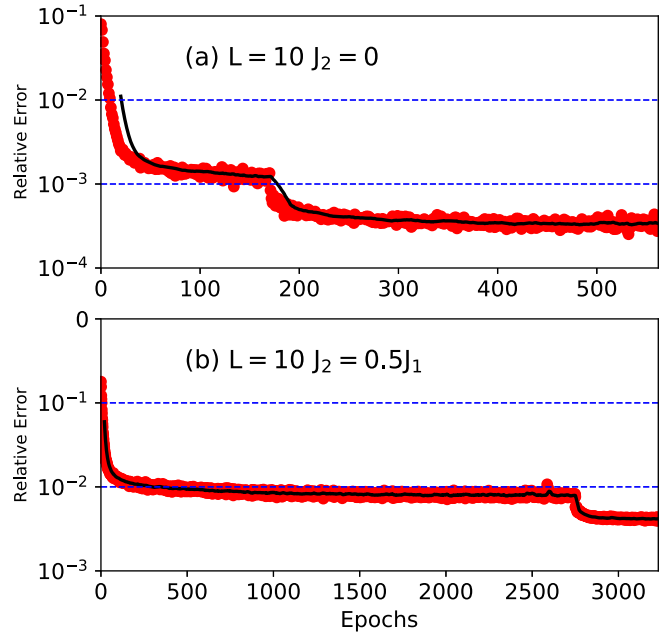

FIG. 3. The optimization of the energy with respect to SR epochs for the PEPS + deep CNN, in the case of (a) $J_2 = 0$ and (b) $J_2 = 0.5$. The relative error is defined as $|(E - E_{\text{best}})/E_{\text{best}}|$, where E_{best} are given in Table II. The SR is first done without enforcing rotational symmetry, and after energy converges, we enforce rotational symmetry on the wave functions, which yields to a sharp decrease of the relative error. The sample number for each SR step is 16 000 without rotational symmetry and 100 000 with rotational symmetry. The energy expectation is averaged over the last ten SR steps, which is denoted by the solid black line.

We find that if we use the PEPS optimized by simple update (SU) under $J_2 = 0.5$ for the sign rule, even with a bond dimension as large as $D = 4$, the energy converges very slowly when further optimizing the CNN. Since it has been shown in Refs. [33,36] that the MPSR is also a good precondition factor for $J_2 = 0.5$, we use the PEPS sign rule obtained from $J_2 = 0$ for the $J_2 = 0.5$ case. The converged energy per site is −0.492 335 for $J_2 = 0.5$, also significantly better than that without the precondition.

We now benchmark the PEPS and deep CNN hybrid wave function for the J_1-J_2 model. We use the same PEPS sign rule as used for the above shallow CNN. The energy convergence with respect to SR steps is depicted in Fig. 3. We start with random parameters for the deep CNN and the wave functions are optimized under fixed PEPS. We first optimize the network without enforcing rotational symmetry. For $J_2 = 0$, the energy converges quickly with respect to the SR steps as shown in Fig. 3(a). After 170 steps, the energy converges to −0.670 697. We then enforce the rotational symmetry, and the energy further reduces to −0.671 330.

The CNN is much more difficult to optimize in the case of $J_2 = 0.5$. As shown in Fig. 3(b), it takes about 2880 SR epochs to converge without enforcing the rotational symmetry, and

TABLE II. Comparison between the ground energies of the spin-1/2 J_1-J_2 model on a 10×10 square lattice, achieved by this work (PEPS+deep CNN) and other NN-based wave-function methods in the literature. The GWF+RBM stands for the RBM-enhanced Gutzwiller projected fermionic wave functions, whereas CNN1 and CNN2 are two convolutional NNs taken from Refs. [33,36], respectively.

	GWF+RBM [21]	CNN1 [33]	CNN2 [36]	Best [55,56]	This work
$J_2 = 0$	−0.67111	−0.67135	−0.671275	−0.671549	−0.671330
$J_2 = 0.5$	−0.49575	−0.49516	−0.494757	−0.49755	−0.495502

the energy per site is −0.493 587. By enforcing the rotational symmetry, the energy further reduces to −0.495 502.

We compare the energies obtained by several state-of-the-art NN methods in Table II. The GWF + RBM wave function [21] is constructed as the product of a Gutzwiller-projected fermionic state and a complex-valued RBM. CNN1 and CNN2 are the two convolutional networks presented in Refs. [33,36], respectively.

The ground state energy for the nonfrustrated model, i.e., $J_2 = 0$ can be obtained to very high accuracy by the stochastic series expansion method [55]. The best ground state energy in the literature for $J_2 = 0.5$ is obtained by a Gutzwiller-projected fermionic wave function improved by the Lanczos iterations [56].

For $J_2 = 0$, our energy is only about 2×10^{-4} higher than the best result. Compared to other NN-based variational wave-function methods, our result is only about 2×10^{-5} higher than the one given by CNN1 [33], but are better than GWF + RBM and CNN2.

For $J_2 = 0.5$, GWF + RBM gives the best results among the NN methods, but is still about 1.8×10^{-4} higher than the best result in the literature [56]. Our energy is about 2.5×10^{-4} higher than the GWF + RBM method, but is lower than the other two CNN methods.

The CNN1 [33] has 3838 complex numbers, and a total of 7676 variational parameters, much more than the 3531 parameters used in our deep CNN. Since the sign structures used in the works are almost identical, our results suggested that the maxpooling is an efficient way to capture the long-range entanglement, and the product of neurons is an efficient way to generate the signs of the wave functions.

We also evaluate the antiferromagetic order parameter

$$S^2(\mathbf{q}) = \frac{1}{N(N+2)} \sum_{i,j} \langle \mathbf{s}_i \cdot \mathbf{s}_j \rangle e^{i\mathbf{q}\cdot(\mathbf{r}_i - \mathbf{r}_j)}, \tag{13}$$

where $\mathbf{q} = (\pi, \pi)$ and $\mathbf{q} = (\pi, 0)$ correspond to the structure factor of Néel order and stripe order, respectively. The spin correlations $\langle \mathbf{s}_i \cdot \mathbf{s}_j \rangle$ are calculated using 10^6 samples. For $J_2 = 0$, we have $S^2(\pi, \pi) = 0.156\,65$ and $S^2(\pi, 0) = 0.004\,96$, whereas for $J_2 = 0.5$ we have $S^2(\pi, \pi) = 0.058\,80$ and $S^2(\pi, 0) = 0.006\,33$. These results are consistent with those given in Refs. [33,36].

In Fig. 4, we compare the spin correlation functions obtained by different CNN structures, in the case of $J_2 = 0.5$,

$$C(r) = \frac{1}{2L^2} \sum_{i,j} \left(\langle \mathbf{s}_{i,j} \cdot \mathbf{s}_{i+r,j} \rangle + \langle \mathbf{s}_{i,j} \cdot \mathbf{s}_{i,j+r} \rangle \right). \tag{14}$$

The results show that the correlation functions obey a power-lay decay. We fit $C(r)$ as $C(r) = \alpha r^{-\gamma} + c_0$, and we plot the correlation functions $G(r) = \alpha r^{-\gamma}$, i.e., the constants have been subtracted. We obtain $\gamma = 2.30$, 2.09, and 2.08 for the shallow CNN, PEPS + shallow CNN, and PEPS + deep CNN, respectively. We see that the correlation function without the PEPS sign structure decays much faster than those with the sign structures, which may cause the errors in the ground state energy.

We remark that this is only a proof-of-principles work where the PEPS sign structures are fixed beforehand, and therefore the ground state energies we obtain are in principle only the upper bound of the energies that can be achieved by this ansatz. A further optimization of the PEPS sign structure along with the optimization of CNN is necessary, especially for the models whose sign rule cannot be reached beforehand. However, because the sign function is a jump function, it makes the optimization of the sign structure very challenging. We leave this problem for future investigations.

IV. SUMMARY

We proposed a variational ansatz for quantum many-particle wave functions which combines two state-of-the-art techniques, i.e., PEPS and deep CNN. In this ansatz, CNN represents the wave-function amplitudes, whereas PEPS provides the sharp changing sign structures which are difficult to be presented by the deep CNN structure. We test this ansatz on the two-dimensional spin-1/2 J_1-J_2 model. We demonstrate that even a PEPS of small bond dimension can present the sign rule very well, and the hybrid structure can achieve a very accurate ground state energy that is competitive with the results of other state-of-the-art neural networks. The further optimization of the PEPS sign structure along with the

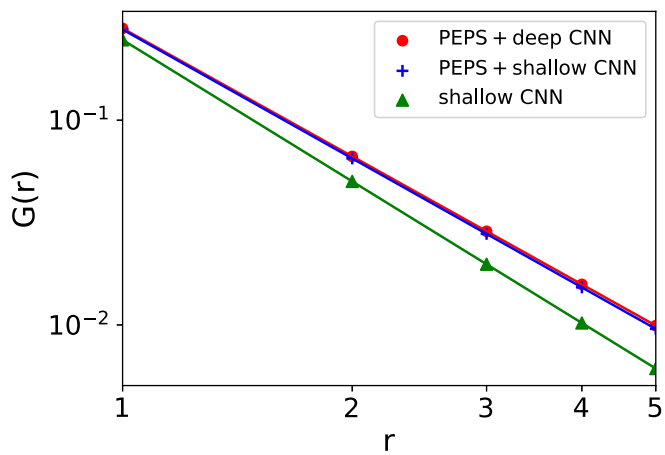

FIG. 4. Correlation function $G(r)$ with respect to distance r for different CNN wave functions, in the case of $J_2 = 0.5$.

optimization of CNN is a promising routine to improve the results and to solve more general models.

ACKNOWLEDGMENTS

X.L. is thankful for inspiring discussions with Li Chen. The implementation of SR was discussed with Giuseppe Carleo. X.L. acknowledges support from the Beijing Outstanding Young Scientist Program, Ministry of Science and Technology Grant No. 2016YFA0301600. L.H. acknowledges support from the Chinese National Science Foundation Grant No. 11774327. S.D. acknowledges the support from China Postdoctoral Science Foundation funded Grant No. 2018M632529. The deep CNN is built by PyTorch. The calculations were done partly on the HPC of USTC, as well as the computational resources in Professor Hui Zhai's group.

[1] G. Carleo, I. Cirac, K. Cranmer, L. Daudet, M. Schuld, N. Tishby, L. Vogt-Maranto, and L. Zdeborová, Machine learning and the physical sciences, Rev. Mod. Phys. **91**, 045002 (2019).

[2] J. Carrasquilla, Machine learning for quantum matter, Adv. Phys.: X **5**, 1797528 (2020).

[3] M. Krenn, J. Handsteiner, M. Fink, R. Fickler, R. Ursin, M. Malik, and A. Zeilinger, Twisted light transmission over 143 km, Proc. Natl. Acad. Sci. U.S.A. **113**, 13648 (2016).

[4] L. Wang, Discovering phase transitions with unsupervised learning, Phys. Rev. B **94**, 195105 (2016).

[5] H. Théveniaut and F. Alet, Neural network setups for a precise detection of the many-body localization transition: Finite-size scaling and limitations, Phys. Rev. B **100**, 224202 (2019).

[6] J. Carrasquilla and R. G. Melko, Machine learning phases of matter, Nat. Phys. **13**, 431 (2017).

[7] N. Sun, J. Yi, P. Zhang, H. Shen, and H. Zhai, Deep learning topological invariants of band insulators, Phys. Rev. B **98**, 085402 (2018).

[8] P. Zhang, H. Shen, and H. Zhai, Machine Learning Topological Invariants with Neural Networks, Phys. Rev. Lett. **120**, 066401 (2018).

[9] Y. Wu, P. Zhang, H. Shen, and H. Zhai, Visualizing a neural network that develops quantum perturbation theory, Phys. Rev. A **98**, 010701(R) (2018).

[10] J. Carrasquilla, D. Luo, F. Pérez, A. Milsted, B. K. Clark, M. Volkovs, and L. Aolita, Probabilistic simulation of quantum circuits with the transformer, arXiv:1912.11052.

[11] L. Huang and L. Wang, Accelerated Monte Carlo simulations with restricted Boltzmann machines, Phys. Rev. B **95**, 035105 (2017).

[12] S. Li, P. M. Dee, E. Khatami, and S. Johnston, Accelerating lattice quantum Monte Carlo simulations using artificial neural networks: Application to the Holstein model, Phys. Rev. B **100**, 020302(R) (2019).

[13] R. Fournier, L. Wang, O. V. Yazyev, and Q. S. Wu, Artificial Neural Network Approach to the Analytic Continuation Problem, Phys. Rev. Lett. **124**, 056401 (2020).

[14] R. Nagai, R. Akashi, and O. Sugino, Completing density functional theory by machine learning hidden messages from molecules, npj Comput. Mater. **6**, 43 (2020).

[15] J. Schmidt, C. L. Benavides-Riveros, and M. A. L. Marques, Machine learning the physical nonlocal exchange-correlation functional of density-functional theory, J. Phys. Chem. Lett. **10**, 6425 (2019).

[16] D.-L. Deng, X. Li, and S. Das Sarma, Quantum Entanglement in Neural Network States, Phys. Rev. X **7**, 021021 (2017).

[17] G. Carleo, Y. Nomura, and M. Imada, Constructing exact representations of quantum many-body systems with deep neural networks, Nat. Commun. **9**, 5322 (2018).

[18] X. Gao and L.-M. Duan, Efficient representation of quantum many-body states with deep neural networks, Nat. Commun. **8**, 662 (2017).

[19] Z.-A. Jia, R. Zhai, Y.-C. Wu, G.-C. Guo, and G.-P. Guo, Quantum neural network states: A brief review of methods and applications, Adv. Quantum Technol. **2**, 1800077 (2019).

[20] K. Choo, A. Mezzacapo, and G. Carleo, Fermionic neural-network states for ab-initio electronic structure, Nat. Commun. **11**, 2368 (2020).

[21] F. Ferrari, F. Becca, and J. Carrasquilla, Neural Gutzwiller-projected variational wave functions, Phys. Rev. B **100**, 125131 (2019).

[22] L. Yang, Z. Leng, G. Yu, A. Patel, W.-J. Hu, and H. Pu, Deep learning-enhanced variational Monte Carlo method for quantum many-body physics, Phys. Rev. Research **2**, 012039(R) (2020).

[23] D. Wu, L. Wang, and P. Zhang, Solving Statistical Mechanics Using Variational Autoregressive Networks, Phys. Rev. Lett. **122**, 080602 (2019).

[24] Z. Cai and J. Liu, Approximating quantum many-body wave functions using artificial neural networks, Phys. Rev. B **97**, 035116 (2018).

[25] G. Carleo and M. Troyer, Solving the quantum many-body problem with artificial neural networks, Science **355**, 602 (2017).

[26] A. Nagy and V. Savona, Variational Quantum Monte Carlo Method with a Neural-Network Ansatz for Open Quantum Systems, Phys. Rev. Lett. **122**, 250501 (2019).

[27] N. Yoshioka and R. Hamazaki, Constructing neural stationary states for open quantum many-body systems, Phys. Rev. B **99**, 214306 (2019).

[28] M. J. Hartmann and G. Carleo, Neural-Network Approach to Dissipative Quantum Many-Body Dynamics, Phys. Rev. Lett. **122**, 250502 (2019).

[29] F. Vicentini, A. Biella, N. Regnault, and C. Ciuti, Variational Neural-Network Ansatz for Steady States in Open Quantum Systems, Phys. Rev. Lett. **122**, 250503 (2019).

[30] Y. Levine, O. Sharir, N. Cohen, and A. Shashua, Quantum Entanglement in Deep Learning Architectures, Phys. Rev. Lett. **122**, 065301 (2019).

[31] X. Liang, W.-Y. Liu, P.-Z. Lin, G.-C. Guo, Y.-S. Zhang, and L. He, Solving frustrated quantum many-particle models with convolutional neural networks, Phys. Rev. B **98**, 104426 (2018).

[32] A. Sfondrini, J. Cerrillo, N. Schuch, and J. I. Cirac, Simulating two- and three-dimensional frustrated quantum systems with string-bond states, Phys. Rev. B **81**, 214426 (2010).

[33] K. Choo, T. Neupert, and G. Carleo, Two-dimensional frustrated J_1-J_2 model studied with neural network quantum states, Phys. Rev. B **100**, 125124 (2019).

[34] A. Voigt and J. Richter, Marshall-Peierls sign rule in frustrated Heisenberg chains, Acta Phys. Pol., A **97**, 979 (2000).

[35] T. Westerhout, N. Astrakhantsev, K. S. Tikhonov, M. I. Katsnelson, and A. A. Bragrov, Generalization properties of neural network approximations to frustrated magnet ground states, Nat. Commun. **11**, 1593 (2020).

[36] A. Szabó and C. Castelnovo, Neural network wave functions and the sign problem, Phys. Rev. Research **2**, 033075 (2020).

[37] F. Verstraete, J. I. Cirac, and V. Murg, Matrix product states, projected entangled pair states, and variational renormalization group methods for quantum spin systems, Adv. Phys. **57**, 143 (2008).

[38] F. Verstraete and J. I. Cirac, Renormalization algorithms for quantum-many body systems in two and higher dimensions, arXiv:cond-mat/0407066.

[39] H. C. Jiang, Z. Y. Weng, and T. Xiang, Accurate Determination of Tensor Network State of Quantum Lattice Models in Two Dimensions, Phys. Rev. Lett. **101**, 090603 (2008).

[40] M. Lubasch, J. I. Cirac, and M.-C. Bañuls, Algorithms for finite projected entangled pair states, Phys. Rev. B **90**, 064425 (2014).

[41] N. Schuch, M. M. Wolf, F. Verstraete, and J. I. Cirac, Computational Complexity of Projected Entangled Pair States, Phys. Rev. Lett. **98**, 140506 (2007).

[42] W.-Y. Liu, S. Dong, C. Wang, Y. Han, H. An, G.-C. Guo, and L. He, Gapless spin liquid ground state of the spin-1/2 J_1-J_2 Heisenberg model on square lattices, Phys. Rev. B **98**, 241109(R) (2018).

[43] W.-Y. Liu, S.-J. Dong, Y.-J. Han, G.-C. Guo, and L. He, Gradient optimization of finite projected entangled pair states, Phys. Rev. B **95**, 195154 (2017).

[44] S.-J. Dong, C. Wang, Y.-J. Han, G.-C. Guo, and L. He, Gradient optimization of fermionic projected entangled pair states on directed lattices, Phys. Rev. B **99**, 195153 (2019).

[45] H. J. Liao, Z. Y. Xie, J. Chen, Z. Y. Liu, H. D. Xie, R. Z. Huang, B. Normand, and T. Xiang, Gapless Spin-Liquid Ground State in the $S = 1/2$ Kagome Antiferromagnet, Phys. Rev. Lett. **118**, 137202 (2017).

[46] P. Corboz, S. R. White, G. Vidal, and M. Troyer, Stripes in the two-dimensional t-J model with infinite projected entangled-pair states, Phys. Rev. B **84**, 041108(R) (2011).

[47] S.-J. Dong, C. Wang, Y.-J. Han, C. Yang, and L. He, Stable diagonal stripes in the t-J model at $\bar{n}_h = 1/8$ doping from fPEPS calculations, npj Quantum Mater. **5**, 28 (2020).

[48] L. P. Kadanoff, *Statistical Physics: Statics, Dynamics and Renormalization* (World Scientific, Singapore, 2000).

[49] K. G. Wilson, The renormalization group: Critical phenomena and the Kondo problem, Rev. Mod. Phys. **47**, 773 (1975).

[50] A. Gelessus, W. Thiel, and W. Weber, Multipoles and Symmetry, J. Chem. Educ. **72**, 505 (1995).

[51] F. Ferrari and F. Becca, Gapless spin liquid and valence-bond solid in the J_1-J_2 Heisenberg model on the square lattice: Insights from singlet and triplet excitations, Phys. Rev. B **102**, 014417 (2020).

[52] Y. Nomura and M. Imada, Dirac-type nodal spin liquid revealed by machine learning, arXiv:2005.14142.

[53] W.-Y. Liu, S.-S. Gong, Y.-B. Li, D. Poilblanc, W.-Q. Chen, and Z.-C. Gu, Gapless quantum spin liquid and global phase diagram of the spin-1/2 J_1-J_2 square antiferromagnetic Heisenberg model, arXiv:2009.01821.

[54] E. Neuscamman, C. J. Umrigar, and G. K.-L. Chan, Optimizing large parameter sets in variational quantum Monte Carlo, Phys. Rev. B **85**, 045103 (2012).

[55] F. Mezzacapo, N. Schuch, M. Boninsegni, and J. I. Cirac, Ground-state properties of quantum many-body systems: Entangled-plaquette states and variational Monte Carlo, New J. Phys. **11**, 083026 (2009).

[56] W.-J. Hu, F. Becca, A. Parola, and S. Sorella, Direct evidence for a gapless Z_2 spin liquid by frustrating Néel antiferromagnetism, Phys. Rev. B **88**, 060402(R) (2013).